Quantum Electronics **36** (11) 990 – 1002 (2006)

REVIEW

PACS numbers: 42.25.Dd; 42.25.Fx; 42.25.Kb; 42.30.Wb
DOI: 10.1070/QE2006v036n11ABEH013338

Numerical simulation of coherent backscattering and temporal intensity correlations in random media

V.L. Kuzmin, I.V. Meglinski

Abstract. **A review of studies on the numerical simulation of coherent effects in random media performed by using exact analytic results is presented. The simulation procedure is based on a comparison of the Monte-Carlo method and the iteration solution of the Bethe – Salpeter equation. The results of calculations of the time correlation function and the interference component of coherent backscattering for scalar and electromagnetic fields are described. The simulation results are compared for the first time with known generalisations of the Milne solution and are in good agreement with experimental data. The interference component of backscattered low-coherent radiation is calculated for the first time. The localisation of backscattered low-coherent laser radiation along the penetration depth is described. The theory and numerical simulation predict, in accordance with the experiment, a considerable broadening of the backscattering peak with decreasing the coherence length, which opens up essentially new possibilities for the use of this effect, especially for medical diagnostics.**

Keywords: *Bethe – Salpeter equation, Monte-Carlo method, coherent backscattering*.

1. Introduction

In the last two decades coherent effects of multiple scattering of laser radiation find expanding applications in studies of the internal structure and dynamics of disordered condensed systems such as colloidal suspensions, foams, aerosols, gels, porous dielectrics, liquid crystals, and various biological tissues [1 – 8]. These effects, which include coherent backscattering (CBS) [9 – 11], spatial and temporal intensity correlations [12, 13], and photon-density waves [14, 15], are caused by the wave nature of light [16 – 18] and are observed in random media despite multiple scattering.

Methods of coherent scattering of laser radiation such as quasi-elastic light scattering, photon correlation, light beating spectroscopy, intensity fluctuation spectroscopy, intensity correlation method, laser correlation photometry, superhigh-resolution Rayleigh spectroscopy, dynamic light scattering, etc. have been used for diagnostics of optically inhomogeneous turbid media beginning from the late 1960s [19 – 22]. Despite their apparent variety, all these methods are based on experiments of the same type, namely, measurements of temporal fluctuations of the scattered radiation intensity in media in which single scattering dominates. The size and velocity of scatterers in the medium are determined by analysing correlations of the intensity fluctuations.

With the development of diffusion-wave spectroscopy (DWS) [23 – 25], which is the extended version of dynamic light scattering applied to multiply scattering media, it became possible to describe the diffusion of field correlations in a random scattering medium [26]. The DWS analysis of the time correlation function (TCF) of the field of multiply scattered radiation allows one to characterise quantitatively the motion of scattering particles in terms of their root-mean-square displacement [25] by the distance of the order of a few nanometres. It has been shown experimentally that the diffusion of time correlations of spatiotemporal fluctuations of light fields in random medium consisting of different spatially separated scattering regions is sensitive to the motion dynamics of scatterers in these regions [27, 28]. The method allows one to distinguish quantitatively variations in the velocity gradient of scatterers in media with the Brownian motion of scatterers [27] and in media with laminar and Poiseuille flows localised in a stationary random medium [28, 29]. It was proposed to use position-dependent TCF measurements to reconstruct the images of dynamic inhomogeneities inside a medium [28, 30, 31]. A dynamic inhomogeneity means a region localised in a random medium in which the motion dynamics of scatterers differs from the dynamics of the rest of the volume.

At present DWS is successfully used for diagnostics of various random media [2 – 5]. However, in our opinion, the most interesting are biomedical applications of DWS. DWS can be used for non-invasive *in vivo* measurements of the bloodstream velocity and microcirculation of blood in the tissue of animals and human [32 – 35], for studying blood microcirculation and activity regions of the brain cortex [36 – 39], and the *in vitro* diagnostics of aggregation and sedimentation of blood samples [40].

Due to the intense recent development of interference optical methods such as optical coherent tomography (OCT) and confocal microscopy and their use for image

V.L. Kuzmin St. Petersburg Institute of Commerce and Economics, Novorossiiskaya ul. 50, 194021 St. Petersburg, Russia; e-mail: vladimir.kuzmin@paloma.spbu.ru;
I.V. Meglinski Department of Physics, N.G. Chernyshevskii Saratov State University, Astrakhanskaya ul. 83, 410026 Saratov, Russia; present address: Cranfield University, School of Engineering, Cranfield, MK43 0AL, UK; e-mail: i.meglinski@Cranfield.ac.uk

Received 23 June 2006; revision received 12 September 2006
Kvantovaya Elektronika **36** (11) 990 – 1002 (2006)
Translated by M.N. Sapozhnikov

visualisation and studies of the internal structure of strongly inhomogeneous biological media [41–43], radiation sources with a small coherence length have received wide applications. In the case of a low coherence of probe laser radiation, the intermediate scattering regime is realised, when the contribution from several low-order scatterings is substantial [44–46], which allows the diagnostics of the state of the surface layers of a medium.

In [47], the dynamic light scattering resolved over the penetration depth for different scattering orders was analysed by using low-coherent interferometry. By analysing the dependence of the intensity spectrum on the optical path, the authors of [47] have found the relation between the contribution from multiple low-coherent scattering and anisotropy parameter and determined in this way the size of scatterers.

CBS was first observed in biological tissues by using ultrashort pulses of duration ~ 100 fs in paper [48] where the scattering pattern resolved in the radiation penetration depth was obtained. It was shown that, as the delay time was increased, the backward scattering peak virtually disappeared. First, it is explained by the fact that the signal is formed with time by contributions from scatterings of increasing orders, whose absolute values decrease, and, second, by the fact that the peak width, which decreases with increasing scattering order, becomes smaller than the angular resolution and, therefore, cannot be observed.

In [49], the CBS amplification was observed at finite time and spatial coherence lengths. It was shown that, when the spatial coherence length became smaller than the transport length, the width of the backward scattering peak could be two orders of magnitude greater than the width of the peak of an infinitely extended monochromatic radiation, which makes the use of low-coherent amplification of backward scattering quite promising for studying biological tissues and, in particular, for diagnostics of cancerous tumours at the earliest stages in epithelium [50].

Coherent effects observed in random media upon multiple scattering are often studied by using stochastic Monte-Carlo simulations [29, 51–60]. The standard simulation technique is based on the radiation intensity transfer. In this case, phase relations between the fields determining the radiation intensity are not simulated and should be taken into account by using a special approach. Monte-Carlo simulations well reproduce the main features of coherent effects such as the universal linear dependence of the TCF on the square root of time [55, 61, 62] and the triangle shape of the CBS peak [52, 54, 56, 59]. However, the results of numerical experiments, especially for the CBS [52, 53, 56, 57], considerably differ from theoretical predictions [63–65].

The theory of multiple scattering in random media, including the theory of coherent and interference effects, is based on the Bethe–Salpeter equation [64]. The well-known exact Milne solution describes scattering of a scalar field from a half-space in the case of isotropic scatterers. The Milne solution was generalised to describe CBS and TCF in the cases of weakly and highly anisotropic scatterings [64–66]. The exact solution was also obtained for Rayleigh scattering [63, 65, 67]. However, these generalised Milne solutions have not been used so far to verify directly the results of numerical simulations. Note in addition that no reliable solution exists yet for an electromagnetic field in the presence of anisotropic scatterers. It is commonly assumed [68] that the scattering anisotropy in the case of a scalar field is simply taken into account by replacing the spatial scale, namely, by passing from the photon mean free path l to the transport length $l^* = l/(1 - \overline{\cos\theta})$, where $\overline{\cos\theta}$ is the scattering angle cosine averaged over the scattering indicatrix. However, numerical simulations in the general case do not confirm [52, 56] that such a scale replacement is sufficient for the electromagnetic field.

In this paper, we discuss a new semianalytic approach involving a comparison of the Monte-Carlo method [69] with the iteration procedure of solution of the Bethe–Salpeter equation represented in the form of a series in scattering orders and based on a direct stochastic calculation of the terms of the iteration series. We show how the standard Monte-Carlo technique is generalised within the framework of the unified approach in numerical simulations of the TCF intensity, CBS, and other coherent effects requiring the consideration of phase shifts. The developed simulation technique allows one to verify for the first time the numerical results by comparing them directly with exact results following from the above-mentioned generalised solutions.

The description of the TCF and CBS proves to be different for scalar and electromagnetic fields. In the case of a scalar field, as assumed within the framework of the diffusion approximation [68], the dependence of CBS on the scattering angle in terms of the transport length l^* as the spatial scale becomes universal. However, for the electromagnetic field this universality is violated: compared to the universal velocity predicted by the diffusion approximation, CBS proves to be weaker with increasing the angle for a smaller scattering anisotropy and stronger for a greater anisotropy. The generalised Milne solution and diffusion approximation in the case of Rayleigh scattering predict that the time dependences of the TCF for polarised and depolarised components of linearly polarised light will be different. We confirm these theoretical results by showing that the polarised and depolarised components are virtually coincident in the case of strong anisotropy.

Note that the Monte-Carlo method was applied for calculating the backscattered radiation intensity, including the coherent component, in [52]. However, the CBS peak intensity for Rayleigh scattering proved to be much smaller than that predicted by the exact solution [63, 65]. In [61], the backscattering of an electromagnetic field was simulated and the depolarisation rate of linearly polarised light was calculated as a function of the number of scattering events. The dependence obtained for Rayleigh scattering coincides with that predicted within the framework of the diffusion approximation [68]; however, in the case of high anisotropy of the single scattering cross section, the result of numerical simulations noticeably differs from the theoretical result.

By comparing the theoretical description of the transfer of correlations based on the Bethe–Salpeter equation or Monte-Carlo method, a method of stochastic simulation of coherent effects taking into account the polarisation of the electromagnetic field was developed in [70]. The calculations performed for Rayleigh scattering within the framework of this model well agree with theoretical results, which suggests that the data obtained for the general case of the anisotropic scattering cross section can be considered reliable.

In systems where CBS and TCF were discovered and find practical applications [5], the weak scattering condition $\lambda/l \ll 1$ is fulfilled, where λ is the incident light wavelength. Under this condition, the coherent components of scattered

radiation are smaller that the incoherent component by the value of the order of $(\lambda/l)^2$ or higher. However, the CBS signal and the TCF at the zero time delay are exactly equal to signals from the incoherent component. As the angular or temporal parameters increase, the contribution of these effects decreases but still remains much greater than the contribution from the rest of the coherent components of scattered radiation, whose smallness is determined by the ratio λ/l. Therefore, there exists the region of parameters where these coherent correlation effects greatly exceed other coherent effects. It is also important that they can be simulated by the methods developed for simulation of the incoherent component. In the general case, beyond the framework of the weak scattering approximation and taking into account the limitedness of light beams, the methods of simulation of coherent and diffraction effects considered here becomes inadequate, and a much more complicated direct simulation of the field is required [71].

The aim of this paper is to review the state of the art in the studies on Bethe–Salpeter-equation-based simulations of coherent backscattering and correlation functions in random media for which the weak-scattering approximation is valid. We present for the first time the field theory of low-coherent backscattering. Numerical calculations based on semianalytic Monte-Carlo simulations developed in [59, 70, 72] well agree with the available data. The localisation of the interference component over the penetration depth has been found, which allows the use of low-coherent backscattering for the optical-path-resolved diagnostics of strongly inhomogeneous media [45–47].

We considered the case of optical radiation scattering in a medium occupying a half-space with a plane interface, which has been often studied theoretically. In section 2, we present general relations for the TCF and the interference backscattering component. In section 3, the method for summation of ladder diagrams is compared with the Monte-Carlo method and the results of simulation of the TCF and CBS for a scalar field are presented. In section 4, the results of simulation performed for linearly polarised light are considered. In section 5, the theory and simulation of the low-coherent backscattered interference component are discussed. In conclusion, the main results are summarised.

2. Transfer of field correlations

The field $\boldsymbol{E}(\boldsymbol{r},t)$ in a random medium experiencing scattering from fluctuations of the dielectric constant $\Delta\varepsilon(\boldsymbol{r})$ is described by the wave equation

$$\boldsymbol{E}(\boldsymbol{r},t)=\boldsymbol{E}_0(\boldsymbol{r},t)+\int \mathrm{d}\boldsymbol{r}\mathrm{d}t'\hat{T}(\boldsymbol{r}-\boldsymbol{r}',t-t')\times\Delta\varepsilon(\boldsymbol{r}')\boldsymbol{E}(\boldsymbol{r}',t'),\tag{2.1}$$

where $\boldsymbol{E}_0(\boldsymbol{r},t)$ is the incident field representing either a plane monochromatic wave or a short pulse with the carrier frequency ω_0; $\hat{T}(\boldsymbol{r},t)=(4\pi)^{-1}(\hat{I}k_0^2+\nabla\times\nabla)r^{-1}\delta(t-r/c)$ is the spatiotemporal Green function of the wave Maxwell equation in a homogeneous medium with a weak dispersion; $k_0=\omega_0/c$; and c is the speed of light. By integrating Eqn (2.1), the scattered field $\delta\boldsymbol{E}(\boldsymbol{r},t)=\boldsymbol{E}(\boldsymbol{r},t)-\boldsymbol{E}_0(\boldsymbol{r},t)$ can be represented by the series

$$\delta\boldsymbol{E}(\boldsymbol{r},t)=\sum_{n=1}^{\infty}\int\prod_{i=1}^{n}\Delta\varepsilon(\boldsymbol{r}_i)\mathrm{d}\boldsymbol{r}_i\hat{T}_\mathrm{s}(\boldsymbol{r}-\boldsymbol{r}_n)\ldots\hat{T}_\mathrm{s}(\boldsymbol{r}_2-\boldsymbol{r}_1)\times\boldsymbol{E}_0\left(\boldsymbol{r}_1,t-\frac{|\boldsymbol{r}-\boldsymbol{r}_n|+R_n}{c}\right),\tag{2.2}$$

where $\hat{T}_\mathrm{s}(\boldsymbol{r})=(\hat{I}k_0^2+\nabla\times\nabla)\exp(\mathrm{i}k_0r)/r$ is the field Green function in a static case;

$$R_n=\sum_{1\leqslant j<n}|\boldsymbol{r}_j-\boldsymbol{r}_{j+1}|$$

is the optical path between n scattering events (from point $\boldsymbol{r}_1$ to point $\boldsymbol{r}_n$). The product of field (2.2) by the complex conjugate field gives the intensity of scattered radiation. Upon static averaging over configurations of scatterers, individual terms of the products of the series contain many-particle averaged fluctuations of the dielectric constant. Due to the phase-difference randomisation appearing upon multiple scattering, only the incoherent (ladder) component remains, which describes the sequence of scattering events for the fields δE and δE^* on the common sequence of fluctuations,

$$\langle\Delta\varepsilon(\boldsymbol{r}_1)\ldots\Delta\varepsilon(\boldsymbol{r}_n)\Delta\varepsilon^*(\boldsymbol{r}'_1)\ldots\Delta\varepsilon^*(\boldsymbol{r}'_m)\rangle_L=\delta_{nm}\prod_{i=1}^{n}\langle\Delta\varepsilon(\boldsymbol{r}_i)\Delta\varepsilon^*(\boldsymbol{r}'_i)\rangle.\tag{2.3}$$

For scattering angles close to the backscattering angle, the interference (cyclic) component [16, 18] formed by the sequences of backscattering (minus the contribution of single scattering) is of the same order of magnitude:

$$\langle\Delta\varepsilon(\boldsymbol{r}_1)\ldots\Delta\varepsilon(\boldsymbol{r}_n)\Delta\varepsilon^*(\boldsymbol{r}'_1)\ldots\Delta\varepsilon^*(\boldsymbol{r}'_m)\rangle_C=\delta_{nm}\prod_{i=1}^{n}\langle\Delta\varepsilon(\boldsymbol{r}_i)\Delta\varepsilon^*(\boldsymbol{r}'_{n-i+1})\rangle.\tag{2.4}$$

Physically, this mean value describes the process in which fields $\delta\boldsymbol{E}$ and $\delta\boldsymbol{E}^*$ are scattered by the same sequence of scatterers passing through them in opposite directions. Other (coherent) contributions from many-particle mean fluctuations of the dielectric constant are small compared to the incoherent component when the weak scattering condition $\lambda/l\ll 1$ is fulfilled, which is valid for dielectric systems under study.

The observed values are the mean strength of the field $\boldsymbol{E}(\boldsymbol{r},t)$ and the higher moments, or correlators, of its fluctuations $\delta\boldsymbol{E}(\boldsymbol{r},t)=\boldsymbol{E}(\boldsymbol{r},t)-\langle\boldsymbol{E}(\boldsymbol{r},t)\rangle$. The second moment, or the coherence function $\langle\delta\boldsymbol{E}^*(\boldsymbol{r}_1,t_1)\delta\boldsymbol{E}(\boldsymbol{r}_2,t_2)\rangle$, in the case of coinciding arguments determines the mean value of the scattered radiation intensity $\langle I(\boldsymbol{r},t)\rangle=\langle|\delta\boldsymbol{E}(\boldsymbol{r},t)|^2\rangle$. The fourth moment determines the spatiotemporal intensity correlation function. In the Gaussian approximation, which makes the main contribution, the correlator of the fourth order in the field is represented as the product of pair correlations

$$\langle I(\boldsymbol{r}_1,t_1)I(\boldsymbol{r}_2,t_2)\rangle=\langle\delta\boldsymbol{E}^*(\boldsymbol{r}_1,t_1)\delta\boldsymbol{E}(\boldsymbol{r}_1,t_1)$$

$$\times \delta \boldsymbol{E}^*(\boldsymbol{r}_2, t_2)\delta \boldsymbol{E}(\boldsymbol{r}_2, t_2)\rangle = \langle I(\boldsymbol{r}_1, t_1)\rangle\langle I(\boldsymbol{r}_2, t_2)\rangle$$

$$+|\langle \delta \boldsymbol{E}^*(\boldsymbol{r}_1, t_1)\delta \boldsymbol{E}(\boldsymbol{r}_2, t_2)\rangle|^2. \quad (2.5)$$

Thus, the observed intensity correlation function in the Gaussian approximation is defined as the product of pair correlators of the field strength. In the case of the incident monochromatic field, the time dependence appears if fluctuations of the dielectric constant describe the dynamics of scatterers, thereby depending on time. When a plane monochromatic wave with the wave vector $\boldsymbol{k}_\mathrm{i}$ is incident on the surface of a medium and the scattered wave with the wave vector $\boldsymbol{k}_\mathrm{b}$ is observed at a large distance, each pair of the fields gives the factor $r^{-2}S$, where S is the illuminated area from which the scattered radiation is detected. Let us define the time correlation function of the field observed at a large distance r from the scattering medium as

$$\langle \delta E_\phi(\boldsymbol{r}, t)\delta E_\phi(\boldsymbol{r}, 0)\rangle = (S/r^2)T_{\phi\beta_1}T_{\phi\beta_2}$$

$$\times C_{\beta_1\beta_2\alpha_1\alpha_2}(t|\boldsymbol{k}_\mathrm{f}, \boldsymbol{k}_\mathrm{i})E^{(0)}_{\alpha_1}E^{(0)}_{\alpha_2}, \quad (2.6)$$

where ϕ and α are polarisations of the scattered and incident light with the wave vectors $\boldsymbol{k}_\mathrm{f}$ and $\boldsymbol{k}_\mathrm{i}$, respectively;

$$\hat{T} = \hat{I} - \frac{\boldsymbol{k}_\mathrm{b} \otimes \boldsymbol{k}_\mathrm{b}}{k^2} \quad (2.7)$$

is the operator making the scattered wave transverse; and $\boldsymbol{E}^{(0)}$ is the incident field amplitude.

Radiation transfer in the case of a monochromatic wave in an inhomogeneous dispersion medium with random fluctuations of the dielectric constant is described by the integral Bethe–Salpeter equation

$$\hat{\Gamma}(\boldsymbol{R}_2, \boldsymbol{R}_1 \,|\, \boldsymbol{k}_\mathrm{b}, \boldsymbol{k}_\mathrm{i}) = k_0^4\widetilde{G}(\boldsymbol{k}_\mathrm{b} - \boldsymbol{k}_\mathrm{i}, t)\delta(\boldsymbol{R}_2 - \boldsymbol{R}_1)\hat{I} + k_0^4$$

$$\times \int \mathrm{d}\boldsymbol{R}_3 \widetilde{G}(\boldsymbol{k}_\mathrm{b} - \boldsymbol{k}_{23})\hat{\Lambda}(\boldsymbol{R}_2 - \boldsymbol{R}_3)\hat{\Gamma}(\boldsymbol{R}_3, \boldsymbol{R}_1 \,|\, \boldsymbol{k}_{23}, \boldsymbol{k}_\mathrm{i}). \quad (2.8)$$

Here, $\Gamma_{\beta_1\beta_2\alpha_1\alpha_2}(\boldsymbol{R}_2, \boldsymbol{R}_1 \,|\, \boldsymbol{k}_\mathrm{b}, \boldsymbol{k}_\mathrm{i})$ is the propagator, or the Green function, of the Bethe–Salpeter equation, which is the fourth-rank tensor. It describes the transfer of two complex conjugate fields, which come to the point $\boldsymbol{R}_1$ with the wave vector $\boldsymbol{k}_\mathrm{i}$ and polarisation described by the Cartesian subscripts α_1 and α_2 and come out from the point $\boldsymbol{R}_2$ with the wave vector $\boldsymbol{k}_\mathrm{b}$ and polarisations β_1 and β_2; $k_\mathrm{s} = k_\mathrm{i} = k = nk_0$; $n = n_1 + in_2$ is the refractive index of a random medium; n_1 and n_2 are the real and imaginary pars of n, respectively; and the photon mean free path $l = (2n_2k_0)^{-1}$ is determined by the imaginary part n_2. The quantity $\boldsymbol{k}_{ij} = k(\boldsymbol{R}_i - \boldsymbol{R}_j)|\boldsymbol{R}_i - \boldsymbol{R}_j|^{-1}$ specifies the wave vector between the ith and jth scattering events. The fourth-rank tensor

$$\Lambda_{\alpha\beta\mu\nu}(\boldsymbol{R}) = \left(\hat{I} - \frac{\boldsymbol{R}\otimes\boldsymbol{R}}{R^2}\right)_{\alpha\mu}\left(\hat{I} - \frac{\boldsymbol{R}\otimes\boldsymbol{R}}{R^2}\right)_{\beta\nu}$$

$$\times \frac{\exp(-R/l)}{R^2} \quad (2.9)$$

is the direct product of the complex conjugate pair of Green functions of the wave Maxwell equation in the far-field region and describes the transformation of a pair of fields with polarisations μ and ν into a pair of fields with polarisations α and β after one scattering event. The Bethe–Salpeter equation is formed by multiplying series (2.2) by a complex conjugate series and subsequent summation and averaging over configurations of random inhomogeneities.

We consider also the case when fluctuations of the dielectric constant describe the dynamics of scatterers $\delta\varepsilon(\boldsymbol{r}) \to \delta\varepsilon(\boldsymbol{r}, t)$. Fluctuations of the dielectric constant become spatially dependent in this case. The Bethe–Salpeter equation describing the transfer of time correlations is formed by multiplying and averaging a complex conjugate pair of fields delayed in time by t. The time factors of the form $\exp(-\mathrm{i}\omega_0 t)$ can be omitted in this case because they are mutually compensated in the construction of products (2.5). The Bethe–Salpeter equation can be easily generalised to describe the transfer of time intensity correlations in a medium with the specified dynamics of scatterers, i.e. in a medium with the Brownian diffusion of inhomogeneities laminar, and turbulent flows, etc. [12, 13] (see also [73]) by including the dependence of the pair of complex conjugate fields on the time shift t to the propagator $\Gamma(\boldsymbol{R}_2, \boldsymbol{R}_1|\,\boldsymbol{k}_\mathrm{b}, \boldsymbol{k}_\mathrm{i}) \to \Gamma(\boldsymbol{R}_2, \boldsymbol{R}_1, t|\,\boldsymbol{k}_\mathrm{b}, \boldsymbol{k}_\mathrm{i})$.

In the weak-scattering approximation ($\lambda \ll l$), which is usually fulfilled in dielectric systems under study, the function $\widetilde{G}(\boldsymbol{q}, t)$ is the Fourier transform of the correlation function of spatiotemporal fluctuations of the dielectric constant,

$$\widetilde{G}(\boldsymbol{q}, t) = \frac{1}{(4\pi)^2}\int \mathrm{d}\boldsymbol{r}\langle \delta\varepsilon(0, 0)\delta\varepsilon(\boldsymbol{r}, t)\rangle \exp(-\mathrm{i}\boldsymbol{q}\boldsymbol{r}). \quad (2.10)$$

The optical theorem relating the single scattering cross section and scattering length l_s plays a key role in problems of multiple scattering [74]. For the electromagnetic field, the optical theorem in the weak-scattering or Born approximation, has the form

$$l_\mathrm{s}^{-1} = \Gamma_\mathrm{R}^{-1}k_0^4\int \mathrm{d}\Omega_\mathrm{s}\widetilde{G}_0(\boldsymbol{k}_\mathrm{s} - \boldsymbol{k}_\mathrm{i}), \quad (2.11)$$

where $\widetilde{G}_0(\boldsymbol{q}) = \widetilde{G}(\boldsymbol{q}, t)$ is the Fourier transform of the static correlator of fluctuations of the dielectric constant; $\Gamma_\mathrm{R} = 2(1 + \overline{\cos^2\theta})^{-1}$ is the Rayleigh factor; and

$$\overline{\cos^2\theta} = \frac{\int \mathrm{d}\Omega_\mathrm{s}\widetilde{G}_0(\boldsymbol{k}_\mathrm{s} - \boldsymbol{k}_\mathrm{i})\cos^2\theta_\mathrm{s}}{\int \mathrm{d}\Omega_\mathrm{s}\widetilde{G}_0(\boldsymbol{k}_\mathrm{s} - \boldsymbol{k}_\mathrm{i})}$$

is the square of the cosine of the scattering angle between the wave vectors $\boldsymbol{k}_\mathrm{i}$ and $\boldsymbol{k}_\mathrm{s}$ averaged over the single scattering cross section.

The photon mean free path l and scattering length l_s are related by the expression

$$l^{-1} = l_\mathrm{s}^{-1} + l_\mathrm{a}^{-1}, \quad (2.12)$$

where l_a is the characteristic absorption length caused by inelastic scattering. For media under study, $l_\mathrm{a} \gg l$ and the ratio l/l_s is close to unity.

Let us define the normalised correlation function of the dielectric constant as

$$p(\boldsymbol{k}_\mathrm{i}-\boldsymbol{k}_\mathrm{b},t)=\frac{\widetilde{G}(\boldsymbol{k}_\mathrm{i}-\boldsymbol{k}_\mathrm{b},t)}{\int\widetilde{G}(\boldsymbol{k}_\mathrm{i}-\boldsymbol{k}_\mathrm{b},0)\mathrm{d}\Omega_s}. \tag{2.13}$$

For $t=0$, this function coincides with the phase function $p_0(\boldsymbol{k}_\mathrm{i}-\boldsymbol{k}_\mathrm{b})=p(\boldsymbol{k}_\mathrm{i}-\boldsymbol{k}_\mathrm{b},0)$ describing the single scattering cross section.

By iterating the Bethe–Salpeter equation with the use of the optical theorem, we obtain the series

$$\begin{aligned}\Gamma(\boldsymbol{R}_2,\boldsymbol{R}_1,t|\boldsymbol{k}_\mathrm{b},\boldsymbol{k}_\mathrm{i})&=\Gamma_\mathrm{R}l_\mathrm{s}^{-1}p(\boldsymbol{k}_\mathrm{i}-\boldsymbol{k}_\mathrm{b},t)\delta(\boldsymbol{R}_2-\boldsymbol{R}_1)\\&+\Gamma_\mathrm{R}^2l_\mathrm{s}^{-2}p(\boldsymbol{k}_\mathrm{b}-\boldsymbol{k}_{21},t)\Lambda(R_{21})p(\boldsymbol{k}_{21}-\boldsymbol{k}_\mathrm{i},t)\\&+\Gamma_\mathrm{R}^3l_\mathrm{s}^{-3}\int\mathrm{d}\boldsymbol{R}_3p(\boldsymbol{k}_\mathrm{b}-\boldsymbol{k}_{23},t)\Lambda(R_{23})p(\boldsymbol{k}_{23}-\boldsymbol{k}_{31},t)\\&\times\Lambda(R_{31})p(\boldsymbol{k}_{31}-\boldsymbol{k}_\mathrm{i},t)+\ldots,\end{aligned} \tag{2.14}$$

which is usually illustrated by a series of ladder diagrams [62].

Let us represent the time correlation function of the field in the form

$$\hat{C}^{(E)}(t\,|\,\boldsymbol{k}_\mathrm{b},\boldsymbol{k}_\mathrm{i})=\hat{C}^{(L)}(t\,|\,\boldsymbol{k}_\mathrm{b},\boldsymbol{k}_\mathrm{i})+\hat{C}^{(V)}(t\,|\,\boldsymbol{k}_\mathrm{b},\boldsymbol{k}_\mathrm{i}), \tag{2.15}$$

where $\hat{C}^{(L)}(t\,|\,\boldsymbol{k}_\mathrm{b},\boldsymbol{k}_\mathrm{i})$ describes the contribution of ladder diagrams, i.e. some incoherent component of scattered radiation and $\hat{C}^{(V)}(t\,|\,\boldsymbol{k}_\mathrm{b},\boldsymbol{k}_\mathrm{i})$ is the interference component called the CBS intensity.

We obtain the scattering intensity in power units from (2.15) by assuming that $t=0$ and multiplying the expression by the geometrical factor Sr^{-2}; then, this expression should be multiplied by the square of the field strength amplitude.

Let us assume that the medium occupies the half-space $z>0$, where z is the Cartesian coordinate normal to the medium boundary. In this case, the ladder and interference components of the coherence function have the form [16, 68]

$$\begin{aligned}C^{(L)}_{\beta_1\beta_2\alpha_1\alpha_2}(t\,|\,\boldsymbol{k}_\mathrm{b},\boldsymbol{k}_\mathrm{i})&=\int\mathrm{d}\boldsymbol{R}_1\mathrm{d}\boldsymbol{R}_2\Gamma_{\beta_1\beta_2\alpha_1\alpha_2}(\boldsymbol{R}_2,\boldsymbol{R}_1,t\,|\,\boldsymbol{k}_\mathrm{b},\boldsymbol{k}_\mathrm{i})\\&\times\exp(-\mu_\mathrm{b}z_2-\mu_\mathrm{i}z_1),\end{aligned} \tag{2.16}$$

$$\begin{aligned}&C^{(V)}_{\beta_1\beta_2\alpha_1\alpha_2}(t\,|\,\boldsymbol{k}_\mathrm{b},\boldsymbol{k}_\mathrm{i})\\&=\int\mathrm{d}\boldsymbol{R}_1\mathrm{d}\boldsymbol{R}_2\left[\Gamma_{\beta_1\alpha_2\alpha_1\beta_2}\left(\boldsymbol{R}_2,\boldsymbol{R}_1,t\,\middle|\,\frac{\boldsymbol{k}_\mathrm{b}-\boldsymbol{k}_\mathrm{i}}{2},\frac{\boldsymbol{k}_\mathrm{i}-\boldsymbol{k}_\mathrm{b}}{2}\right)\right.\\&\left.-k_0^4\widetilde{G}(\boldsymbol{k}_\mathrm{b}-\boldsymbol{k}_\mathrm{i},t)\delta(\boldsymbol{R}_2-\boldsymbol{R}_1)\delta_{\alpha_1\beta_1}\delta_{\alpha_2\beta_2}\right]\exp[-(z_2+z_1)\\&\times(\mu_\mathrm{b}+\mu_\mathrm{i})/2+\mathrm{i}(\boldsymbol{k}_\mathrm{b}+\boldsymbol{k}_\mathrm{i})_\perp(\boldsymbol{R}_2-\boldsymbol{R}_1)_\perp],\end{aligned} \tag{2.17}$$

where the subscript $\perp$ denote the component perpendicular to the normal to the medium boundary; $\mu_\mathrm{i}=(l\cos\theta_\mathrm{i})^{-1}$; $\mu_\mathrm{b}=(l\cos\theta_\mathrm{s})^{-1}$; θ_i is the angle of incidence; and θ_s is the scattering angle. It is easy to see that in the case of backward scattering ($\boldsymbol{k}_\mathrm{b}=-\boldsymbol{k}_\mathrm{i}$), the polarised component $\hat{C}^{(V)}(t\,|\,\boldsymbol{k}_\mathrm{b},\boldsymbol{k}_\mathrm{i})$ of the interference contribution exactly coincides with the polarised component $\hat{C}^{(L)}(t\,|\,\boldsymbol{k}_\mathrm{b},\boldsymbol{k}_\mathrm{i})$ of the main, incoherent contribution before the subtraction of the single-scattering contribution from it; the depolarised components do not coincide.

In the absence of the time shift of the observed fields ($t=0$), the ladder component (2.16) determines the main, incoherent component of the scattered radiation intensity

$$I_{\beta_1\beta_2\alpha_1\alpha_2}(\boldsymbol{k}_\mathrm{b},\boldsymbol{k}_\mathrm{b})=C^{(L)}_{\beta_1\beta_2\alpha_1\alpha_2}(0\,|\,\boldsymbol{k}_\mathrm{b},\boldsymbol{k}_\mathrm{i}). \tag{2.18}$$

In the general case, the incoherent component specifies the field TCF. The interference component (2.18) for $t=0$ describes the incoherent backscattering component

$$I^{(\mathrm{CBS})}_{\beta_1\beta_2\alpha_1\alpha_2}(\theta_s)=C^{(V)}_{\beta_1\beta_2\alpha_1\alpha_2}(0\,|\,\boldsymbol{k}_s,\boldsymbol{k}_\mathrm{i}) \tag{2.19}$$

and its angular dependence. To avoid cumbersome expressions, we will restrict ourselves below to the case of normal incidence and nearly backward scattering.

3. Simulation of a series in scattering orders. The scalar field

Let us compare the procedure of analytic summation of ladder diagrams and the Monte-Carlo method. Consider first a scalar field. In the case of a scalar field, the tensor $\hat{\Lambda}(\boldsymbol{R})$ is replaced by the scalar function $\Lambda_0(\boldsymbol{R})=R^{-2}\times\exp(-R/l)$, and the Rayleigh factor – by unity.

The analytic calculation is complicated because integrals over $\boldsymbol{R}_\mathrm{i}$ cannot be uncoupled because phase functions depend on the mutual arrangement of scattering particles. The numerical simulation uncouples this chain by specifying randomly at each step the direction and mean free path of a photon packet.

Due to the normalisation of the phase function

$$\int p_0(\boldsymbol{k}_\mathrm{i}-\boldsymbol{k}_\mathrm{b})\mathrm{d}\Omega=1 \tag{3.1}$$

the statistical weight of the photon packet does not change after each scattering event. The packet weight is preserved in the theoretical description according to the optical theorem. Indeed, $\int\Lambda_0(R)\mathrm{d}\boldsymbol{R}=4\pi l$, and the expansion parameter of the iteration series (2.14) is

$$l_\mathrm{s}^{-1}\int\mathrm{d}\Omega_n\int\mathrm{d}R_{\mathrm{i}+1}\Lambda_0(\boldsymbol{R}_{\mathrm{i}+1}-\boldsymbol{R}_\mathrm{i})p_0(\boldsymbol{k}_{\mathrm{i}+1}-\boldsymbol{k}_\mathrm{i})=l/l_s. \tag{3.2}$$

Note that the form of the propagator $\Lambda_0(\boldsymbol{R})$ results in the representation of the sampling of mean free paths with the help of the Poisson distribution [69]. In the absence of absorption, the ratio l/l_s is equal to unity, which demonstrates the preservation of the photon packet weight. It is the condition $l/l_\mathrm{s}=1$ that makes the method of successive approximations invalid in analytic calculations for solving the Bethe–Salpeter equation.

We used the Henyey–Greenstein function [75] as the phase function. Within the framework of the semianalytic Monte-Carlo method developed in [70], the main, incoherent component of the scattered intensity is represented as a series in scattering orders:

$$I(\mu_\mathrm{b},\mu_\mathrm{i})=\sum_{n<n_\mathrm{sc}}I_n(\mu_\mathrm{b},\mu_\mathrm{i}), \tag{3.3}$$

where

$$I_n(\mu_b, \mu_i) = \frac{1}{N_{ph}} \sum_{i=1}^{N_{ph}} W_n^{(i)} \exp(-\mu_b z_n^{(i)}) \quad (3.4)$$

is the contribution of paths containing n scattering events as the mean of the sampling N_{ph} of incident photons; $W_n^{(i)}$ and $z_n^{(i)}$ are the statistical weight and distance to the medium boundary, respectively, for the ith photon that has experienced n scattering events.

The statistical weight $W_n^{(i)}$ is determined by the contribution of the chain of integrals: $\int d\boldsymbol{r}_j \Lambda(\boldsymbol{r}_{j+1} - \boldsymbol{r}_j) p(\boldsymbol{q}_j)$. After the change of the integration variable $r_j = -l \ln \xi_j$, which is usually interpreted as the Poisson distribution of random photon mean free paths, the spatial integral over the infinite interval transforms to the integral over the interval [0, 1]:

$$\int_0^\infty r_j^2 dr_j \Lambda(r_j) = \int_0^1 d\xi_j.$$

This integral was calculated as the statistical mean over the sampling of values ξ_i specified by a random number generator. The phase function in the intrinsic coordinate system depends only on the scattering angle: $p(\boldsymbol{q}_j) = p(\cos\theta_j)$. Then, after the substitution

$$\int_{-1}^{\upsilon_j} p(\cos\theta_j) d(\cos\theta_j) \to \upsilon_j$$

integrals over polar angles are calculated as the sampling mean over random values υ_j distributed uniformly in the interval [0, 1].

The simulation accuracy in this method can be easily controlled by comparing the obtained results with analytic results, which can be obtained for the lower orders. Thus, the contributions of single and double isotropic scatterings $I_{single} = 1/2$ and $I_{double} = \ln\sqrt{2} = 0.346$, which are known theoretically, are reproduced almost exactly; for the total radiation intensity, we have $I \approx 4.2$ for $n_{sc} = 10^4$, in good accordance with the Milne result $I_{Milne} = 4.227$ [64]. Hereafter, by restricting ourselves to the case of normal incidence and nearly backward scattering, we omit the arguments μ_b and μ_i for brevity. For strong anisotropic scattering ($\overline{\cos\theta} = 0.9$), we have $I \approx 4.5 \pm 0.3$ for $n_{sc} = 10^5$, which corresponds to the theoretical value $I = 4.88$ obtained in the limit $\overline{\cos\theta} \to 1$ [64].

A comparison of the theoretical approach based on the Bethe–Salpeter equation and the Monte-Carlo method makes it possible to generalise the latter to simulate the coherent effects of multiple scattering. Usually, time correlations are studied by considering only the main, incoherent contribution. The TCF of the field is defined as

$$g_1(t) = \frac{C^{(L)}(t \mid -\boldsymbol{k}_i, \boldsymbol{k}_i)}{C^{(L)}(0 \mid -\boldsymbol{k}_i, \boldsymbol{k}_i)}.$$

By neglecting non-Gaussian, long-range components (see [76]), the intensity TCF is represented as the square of the field TCF: $g_2(t) = 1 + g_1^2(t)$.

The calculation of the TCF differs from the intensity calculation by the fact that the direction of a photon packet upon scattering is determined not by the phase function but its generalisation $p(\boldsymbol{k}_j - \boldsymbol{k}_{j-1}, t)$ depending on the time shift t. In most known applications [23, 24], the diffusion mechanism of the time evolution of dynamic inhomogeneities is studied, when the TCF of the intensity fluctuations can be represented as the product of the statistical correlator and the exponential:

$$p(q, t) \approx p_0(q) \exp(-D_s q^2 t), \quad (3.5)$$

where D_s is the self-diffusion coefficient. Thus, the TCF calculated by the Monte-Carlo method has the form

$$g_1(t) = \frac{1}{N_{ph}} \sum_n \sum_i W_n^{(i)} \exp\left[-2 \sum_{j=1}^n \frac{t}{\tau} \times (1 - \cos\theta_j) - z_n^{(i)}/l \right], \quad (3.6)$$

where $\tau = (D_s k^2)^{-1}$ is the characteristic time of the Brownian diffusion of scatterers by the distance λ; and θ_j is the scattering angle in the jth scattering event.

For isotropic scattering, the exact Milne solution is known, which makes it possible to control the simulation results. The ratio of the total intensity of backscattered radiation to that of single scattering obtained in the case of the exact solution is $I/I_{single} = 8.455$ (see [64]). The simulation method described above reproduces this value with accuracy of no less than to four decimal places for the sampling volume of the order of 10^5. To reduce the simulation time, the contribution from photons for which the distance from the entrance to exit point exceeds the mean free path l by a few tens of times was calculated theoretically in the diffusion approximation, while the contribution of photons coming out at a distance smaller than the distance indicated above was found by using simulations described in the paper.

Figure 1 presents the field TCFs simulated for isotropic ($\overline{\cos\theta} = 0$) and strongly anisotropic ($\overline{\cos\theta} = 0.9$) scatterings. One can see that the initial slope in the dependence on $\sqrt{t/\tau}$ can be considered quite universal and independent of

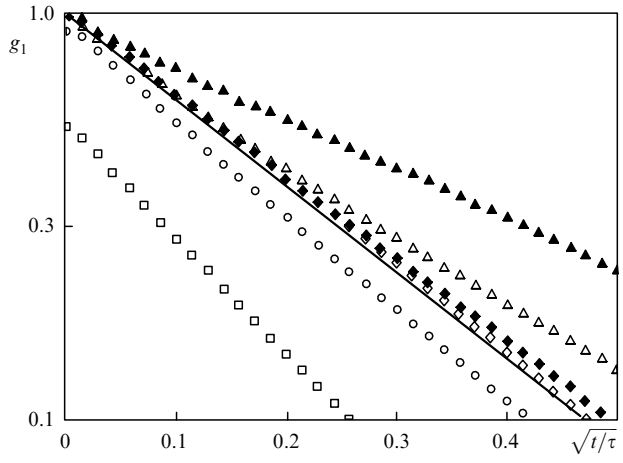

Figure 1. Dependences of the field TCF g_1 on $\sqrt{t/\tau}$. Scalar field: (△) isotropic scattering ($\overline{\cos\theta} = 0$), (◇) anisotropic scattering ($\overline{\cos\theta} = 0.9$); electromagnetic field, polarised component: (▲) Rayleigh scattering ($\overline{\cos\theta} = 0$), (◆) anisotropic scattering ($\overline{\cos\theta} = 0.9$); depolarised component normalised to the intensity of the incoherent component of the polarised component: (□) Rayleigh scattering ($\overline{\cos\theta} = 0.9$), (○) anisotropic scattering ($\overline{\cos\theta} = 0.9$); solid curve is the approximation $\exp(-2\sqrt{6t/\tau})$. The stochastic sampling power is $N_{in} = 10^5$, the maximum number of considered scattering events is $n = 50000$.

the anisotropy parameter $\overline{\cos\theta}$. This is consistent with the theoretical prediction [64, 65] and known numerical results [55, 61, 62]. Note that for ($\overline{\cos\theta} = 0.9$), the obtained curve virtually reproduces the experimental curve (see Fig. 2 in [24]).

An important feature of the simulation results is that they almost do not change after the replacement $\sum_j^n \cos\theta_j \to n\overline{\cos\theta}$ in (3.6). For short times ($t \ll \tau$), the main contribution to scattered radiation and field correlations is determined by longer paths containing a great number of scattering events n, and therefore such a replacement is the replacement of the mean of the exponential describing the phase shift due to the time shift by the exponential of the mean. Thus, the exponential phase factor is the exponential function of the scattering order. Such a dependence considerably reduces the simulation time because it allows one to calculate simply the n-order contribution to the radiation intensity and then to multiply it by the phase factor

$$g_1(t) = \sum_{n=1}^{n_{sc}} I_n \exp[-2n\frac{t}{\tau}(1 - \overline{\cos\theta})]. \tag{3.7}$$

For long times $t/\tau \sim 1$, the mean of the exponential is not equal to the exponential of the mean; however, the multiplicative dependence on the scattering order is preserved.

The obtained TCF dependence is well described by the expression

$$g_1(t) \propto \exp(-\gamma\sqrt{6t/\tau}) \tag{3.8}$$

proposed in [24].

The TCF decrease rate in dimensionless units t/τ, which weakly depends on the properties of a medium, strongly depends on the experimental geometry. On passing from plane waves to a point source or detector, the decrease rate of correlations becomes smaller. This is explained by the fact that the relative contribution of longer optical paths in the case of plane waves increases, resulting in a faster decrease of the TCF.

Note that the intensity of the interference component of backward scattering (2.17) differs from that of the incoherent component by the factor

$$S_n^{(i)} = \exp[(\boldsymbol{k}_b + \boldsymbol{k}_i)_\perp(\boldsymbol{R}_n^{(i)} - \boldsymbol{R}_1^{(i)})_\perp].$$

Taking into account the translation invariance with respect to coordinates $\boldsymbol{R}_\perp$, this factor can be replaced by $\cos[\boldsymbol{q}_\perp \times(\boldsymbol{R}_1 - \boldsymbol{R}_2)_\perp] \approx \cos[k(x_n - x_1)\theta_s]$, where the x axis determines the direction of angular scanning. By calculating the TCF intensity, the weight of each ith photon with the wave vector $\boldsymbol{k}_b$ incident on the medium boundary at a distance of $|(\boldsymbol{R}_S^{(i)} - \boldsymbol{R}_D^{(i)})_\perp|$ from the entrance poit $\boldsymbol{R}_S^{(i)}$ ($\boldsymbol{R}_D^{(i)}$ is the detection point) should be multiplied by the factor $\cos[\boldsymbol{q}_\perp(\boldsymbol{R}_S^{(i)} - \boldsymbol{R}_D^{(i)})_\perp]$ and summed over all photons. As a result, we obtain for the TCF peak

$$I^{(CBS)}(\theta_s) = \frac{1}{N_{ph}} \sum_n \sum_i W_n^{(i)} \cos[\boldsymbol{q}_\perp(\boldsymbol{R}_S^{(i)} - \boldsymbol{R}_D^{(i)})_\perp] - I_{single}.$$

The height, or amplification, of the backscattering peak is

$$h^{(CBS)} = \frac{2I - I_{single}}{I},$$

where I is the incoherent component intensity. The calculation for isotropic scattering gives $h^{(CBS)} = 1.87$, in good agreement with the value $h_{theor}^{(CBS)} = 1.88$ obtained from the generalised Milne solution [64]. For $\overline{\cos\theta} = 0.9$, we have $h^{(CBS)} = 1.99$, which also well agrees with the expected theoretical value $h^{(CBS)} = 2$ for $\overline{\cos\theta} \to 1$.

Figure 2 presents the CBS component normalised to the incoherent backscattering component as a function of the universal angular coefficient $kl^*\theta_s$. The obtained angular dependences prove to be universal within a rather broad angular region expressed in the $kl^*\theta_s$ units.

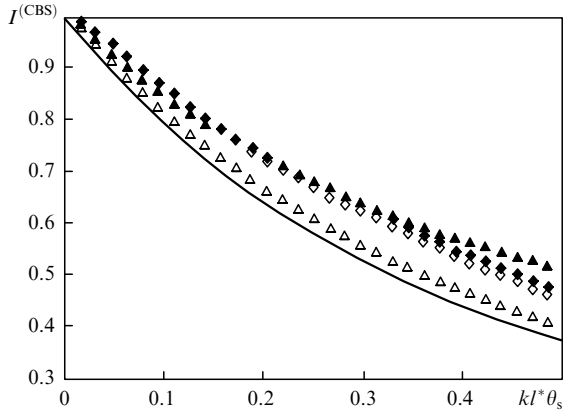

Figure 2. Dependences of the normalised CBS component on the universal angular variable $kl^*\theta_s$. Scalar field: (△) isotropic scattering ($\overline{\cos\theta} = 0$), (◇) anisotropic scattering ($\overline{\cos\theta} = 0.9$); electromagnetic field, polarised component t: (▲) Rayleigh scattering ($\overline{\cos\theta} = 0$), (◆) anisotropic scattering ($\overline{\cos\theta} = 0.9$); solid curve is the diffusion approximation [see (3.9)].

In the diffusion approximation, the angular dependence of CBS has the form [68]

$$I^{(CBS)} \sim \frac{1}{(1 + kl^*\theta_s)^2}\left[1 + \frac{1 - \exp(-2zkl^*\theta_s)}{kl^*\theta_s}\right]. \tag{3.9}$$

One can see from Fig. 2 that deviations of the CBS curves from the curve obtained in the diffusion approximation increase with increasing scattering angle; however, expression (3.9) is valid only in the region of small angles.

In problems of multiple scattering, scattered radiation is mainly determined by the incoherent component. Coherent components have the smallness order λ/l compared to the incoherent component. When the characteristic parameters $kl^*\theta$ for CBS and t/τ for the TCF for effects under study are still greater than the smallness parameter λ/l, these effects can be considered separately by neglecting other coherent or diffraction components and using simulation methods based on the generalisation of simulation of the incoherent component.

4. Coherent effects in an electromagnetic field

Because polarised light is completely depolarised due to multiple scattering, the study can be performed within the

framework of a scalar field. However, due to lower-order contributions in backward scattering, the scattered light remains partially polarised. Experiments [14, 24, 77, 78] have demonstrated a considerable role of polarisation in backscattering.

The problem of multiple scattering by point Rayleigh particles was solved by generalising the Milne solution to the case of an electromagnetic field in papers [63, 65, 67, 79–81]. In [67, 79], the vector transfer equation was solved for strictly backward scattering taking into account the interference component, and in [63, 80] the angular dependences of the CBS peak were calculated taking polarisation into account. In [81], the solution for the TCF was obtained, and in [65] this solution was generalised to scatterers of a finite size.

In the case of an electromagnetic wave, it is also necessary to control variations in the field direction, characterised by the polarisation vector, along a random path of a photon packet. According to (2.9), this requires the calculation of the result of the action of a chain of operators [68]

$$\prod_{j=1}^{n}[\hat{I}-(\boldsymbol{R}_j-\boldsymbol{R}_{j-1})\otimes(\boldsymbol{R}_j-\boldsymbol{R}_{j-1})|\boldsymbol{R}_j-\boldsymbol{R}_{j-1}|^{-2}] \tag{4.1}$$

on the incident field. Except the weight, the initial polarisation is specified, which is determined in the general case by three Cartesian components. Let the initial polarisation vector of each photon packet for linearly polarised incident radiation be determined by a set of three numbers, $\boldsymbol{P}_{\rm in}=(1;\,0;\,0)$, i.e. the incident field is polarised along the x axis.

Because the field polarisation changes upon scattering, it is necessary, apart from the usual procedure of stochastic determination of the photon direction after a collision event taking the phase function into account, to calculate a new vector $\boldsymbol{P}_{j+1}$ from the previous polarisation vector $\boldsymbol{P}_j$ in each scattering event. Let us assume that a photon packet propagating from the point $\boldsymbol{R}_{\rm S}$ to $\boldsymbol{R}_{\rm D}$ experiences n scattering events; then, the photon packet will arrive at the observation point $\boldsymbol{R}_{\rm D}$ with the polarisation vector

$$\boldsymbol{P}_{\rm out}=\prod_j\left[\hat{I}-\frac{(\boldsymbol{R}_{j+1}-\boldsymbol{R}_j)\otimes(\boldsymbol{R}_{j+1}-\boldsymbol{R}_j)}{|\boldsymbol{R}_{j+1}-\boldsymbol{R}_j|^2}\right]\boldsymbol{P}_{\rm in}. \tag{4.2}$$

Let W_i be the statistical weight of a 'scalar' ith photon arrived at the point $\boldsymbol{R}_{\rm D}^i$. Then, after summation over all detected photons $N_{\rm ph}$ for the polarised and depolarised components of the scattered radiation intensity (the subscript out is omitted for brevity), we obtain

$$I_{\rm pol}=I_{XX}=\sum_{i=1}^{N_{\rm ph}}W_iP_{i\,x}^2\Gamma_{\rm R}^{n_i},$$
$$I_{\rm depol}=I_{YX}=\sum_{i=1}^{N_{\rm ph}}W_iP_{i\,y}^2\Gamma_{\rm R}^{n_i}. \tag{4.3}$$

These expressions describe the incoherent contribution $I_{\beta\alpha}=C^{(\rm L)}_{\beta\beta\alpha\alpha}(0|\boldsymbol{k}_{\rm b},\boldsymbol{k}_{\rm i})$ of ladder diagrams.

In the case of the electromagnetic field, the polarisation vector continues to fluctuate strongly even for very large volumes of the statistical sampling, $\sim 10^6$ and more. In [68], the dependence of the depolarisation rate on the number n of scattering events was analysed in the diffusion approximation. For Rayleigh scattering, the degree of residual polarisation after n scattering events has the form [68]

$$P(n)=\frac{I_{\rm pol}(n)-I_{\rm depol}(n)}{I_{\rm pol}(n)+I_{\rm depol}(n)}=\frac{3(0.7)^{n-1}}{2+(0.7)^{n-1}}.$$

The number of scattering events is proportional to the found path: $n\propto s/l_{\rm s}$.

Figure 3 presents the degree of polarisation P calculated as a function of the number n of scattering events. Because $n\propto s/l_{\rm s}$ and the path length is proportional to the flight time, the dependences shown in Fig. 3 also demonstrate the law of spreading of an ultrashort light pulse in a strongly inhomogeneous medium. One can see that depolarisation indeed exponentially decreases with increasing optical path; however, the decrease rate differs from that predicted in the diffusion approximation. As anisotropy increases, the characteristic depolarisation length increases because at large values of $\overline{\cos\theta}$ the number of collisions that a photon should experience to change noticeably its direction and, hence, polarisation will be $(1-\overline{\cos\theta}\,)^{-1}$ times greater than in the isotropic case. For the number of scattering events $n\sim 20$ for Rayleigh scattering and $n\sim 100$ for the anisotropic medium, the scatter in P becomes considerable. This is explained by the fact that products of the odd number of components of the polarisation vector along components perpendicular to the normal to the surface are theoretically equal to zero, however, the stochastic result strongly fluctuates.

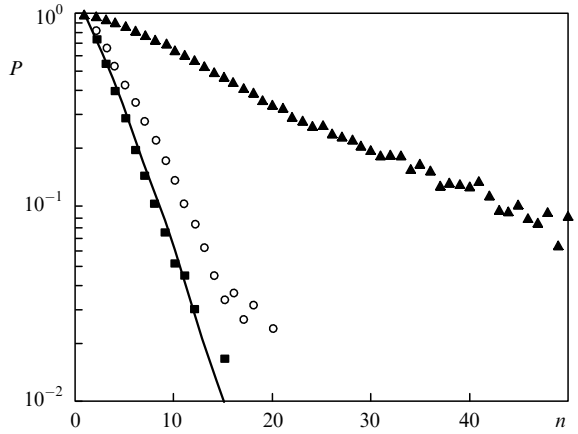

Figure 3. Dependences of the depolarisation degree P of the incident light on the number n of scattering events for Rayleigh scattering ($\overline{\cos\theta}=0$) (■) and anisotropic scattering ($\overline{\cos\theta}=0.5$) (○) and $\overline{\cos\theta}=0.9$ (▲).

In this case, because the polarised and depolarised components become almost equal for $n>n_0$, to reduce the calculation time, it is reasonable to set them equal to half the contribution of the scalar field intensity

$$I_{\rm pol}(n)=I_{\rm depol}(n)=\frac{1}{2}I_{\rm scal}(n).$$

Formally, this means that we make the substitution $P_\alpha^2\Gamma_{\rm R}^{n_i}\to\frac{1}{2}$ for $n>n_0$ in (4.3). For paths with the number

of scattering events smaller than $n_0 \sim 10$ for Rayleigh scattering and $n_0 \sim 100$ for the anisotropic medium, the calculation was performed by the method described above.

The verification of the results of this approach compared to the known exact theoretical results for the case of point scatterers showed the following. In the case of normal incidence of light and Rayleigh scattering at an angle of 180°, the exact solution [65, 81] obtained by generalising the Milne solution for the electromagnetic field gives the ratio of the polarised and depolarised components of the incoherent component $I_{\rm pol}/I_{\rm depol} \approx 1.92$, whereas the numerical calculation gives $I_{\rm pol}/I_{\rm depol} \approx 1.94$. The known ratio of the polarised and depolarised components of scattered radiation allows one to find the residual polarisation of the incoherent backscattering component. The generalisation of the Milne solution gives [63, 65, 81] $(I_{\rm pol} - I_{\rm depol})/(I_{\rm pol} + I_{\rm depol}) \approx 0.31$, while the simulation result is 0.326. A close value (0.33) was numerically obtained in [61].

Let us define the peak intensity of the polarised CBS component as

$$h_{\rm pol}^{\rm (CBS)} = \frac{2I_{\rm pol} - I_{\rm single}}{I_{\rm pol}}.$$

The theoretical value is $h_{\rm pol}^{\rm (CBS)} \approx 1.75$ [63, 65, 81]. The simulation performed in [52] gives the value $h_{\rm pol}^{\rm (CBS)} \approx 1.4$, which strongly differs from the theoretical value. In [56], the value $h_{\rm pol}^{\rm (CBS)} \approx 1.69$ was obtained, whereas we obtained by our method the value $h_{\rm pol}^{\rm (CBS)} \approx 1.746$ which much better agrees with the theoretical result.

The electromagnetic field was simulated numerically by using the expressions

$$g_{\rm pol}^{(1)}(t) = \sum_{i=1}^{N_{\rm ph}} W_i P_{i\,x}^2 \Gamma_{\rm R}^{n_i} \exp\left[-2\frac{t}{\tau} n_i \left(1 - \frac{1}{n_i} \sum_{j}^{n_i} \cos\theta_j \right) \right], \tag{4.4}$$

$$g_{\rm depol}^{(1)}(t) = \sum_{i=1}^{N_{\rm ph}} W_i P_{i\,y}^2 \Gamma_{\rm R}^{n_i} \exp\left[-2\frac{t}{\tau} n_i \left(1 - \frac{1}{n_i} \sum_{j}^{n_i} \cos\theta_j \right) \right],$$

where $P_{i\alpha}$ is the polarisation vector of the ith photon with polarisation α appearing due to the action of a sequence of n_i tensor operators of type (4.1); and θ_j is the scattering angle in the jth scattering event.

Figure 1 shows the results of simulation of the polarised and depolarised TCF components for Rayleigh scattering and strongly anisotropic, elongated forward indicatrix. In the case of Rayleigh scattering, the theory [63, 65] predicts the slopes of the polarised and depolarised components equal to $\gamma_{\rm pol} \approx 1.44$ and $\gamma_{\rm depol} \approx 2.75$, respectively. Calculations performed in the diffusion approximation [78] give the values $\gamma_{\rm pol} \approx 1.6$ and $\gamma_{\rm depol} \approx 2.7$, which are close to experimental values $\gamma_{\rm pol} \approx 1.6 \pm 0.1$ and $\gamma_{\rm depol} \approx 2.8 \pm 0.2$. Our results ($\gamma_{\rm pol} \approx 1.5 \pm 0.1$ and $\gamma_{\rm depol} \approx 2.6 \pm 0.2$) well agree with these data. Note that the dependence of the sum of polarised and depolarised components, i.e. the TCF of nonpolarised light on $\sqrt{t/\tau}$ is close to the curve obtained by simulating the TCF.

We also calculated the angular dependence of the polarised CBS component. The results for Rayleigh and strongly anisotropic scatterings are presented in Fig. 2. One can see that these dependences considerably differ from the curve obtained in the diffusion approximation for a scalar field. In the case of a weak anisotropy, the CBS peak decreases slower than predicted by expression (3.9), whereas in the case of a strong anisotropy ($\overline{\cos\theta} = 0.9$), the CBSs for scalar and electromagnetic fields virtually coincide.

In the case of a scalar field, the obtained dependences are universal in units $kl^*\theta_{\rm s}$, as should be within the framework of the diffusion approximation. However, this universality is violated for an electromagnetic field. In this case, the curves describing the CBS as a function of $kl^*\theta_{\rm s}$ are considerably different for media with different anisotropy parameters. Thus, in the case of the scalar field, the angular dependences of the CBS are close to each other, whereas for the electromagnetic field they are coming apart with increasing anisotropy.

5. Simulation of the interference component of backscattered low-coherent radiation

In the case of a monochromatic wave with an infinite coherence length, the interference component of backscattered radiation is exactly equal to the incoherent component minus the contribution of single scattering [10, 11, 68]. The contribution of the interference component for low-coherent radiation proves to be considerably smaller than the incoherent contribution (being only a few percent), however, it is the interference component that provides the resolution over the penetration depth in a turbid medium.

We represent the field of a short light pulse, which did not experience yet scattering by random inhomogeneities, in the form of the spectral expansion in plane waves

$$E_0(\boldsymbol{r}, t) = \int_{-\infty}^{\infty} {\rm d}\omega f(\omega - \omega_0) \exp(-{\rm i}\omega t + {\rm i}\boldsymbol{kr}). \tag{5.1}$$

Here, ω is the frequency; $\boldsymbol{k}$ is the wave vector satisfying the dispersion relation $k^2 c_0^2 - n^2(\omega)\omega^2 = 0$; $n(\omega)$ is the refractive index of the medium by neglecting random inhomogeneities or scattering particles; and c_0 is the speed of light in vacuum. We assume that the spectral distribution $f(\omega)$ is described by a Gaussian of width Ω centred at frequency ω_0:

$$f(\omega - \omega_0) = \frac{1}{\Omega} \exp\left[-\frac{(\omega - \omega_0)^2}{2\Omega^2} \right]. \tag{5.2}$$

The refractive index of the medium weakly changes within the frequency band $\omega_0 \pm \Omega$; by assuming that $k \approx n(\omega_0)\omega/c_0$, where $n(\omega_0)$ is the refractive index at frequency ω_0, and integrating by frequencies in (5.1), we obtain the expression for the field in the form of a spatiotemporal pulse

$$E_0(\boldsymbol{r}, t) = \exp(-{\rm i}\omega_0 t + {\rm i}\boldsymbol{kr}) \exp\left[-\frac{\Omega^2 (t - r/c)^2}{2} \right], \tag{5.3}$$

where $c = c_0/n(\omega_0)$ is the speed of light in the medium. The field is depolarised due to multiple scattering, which makes it possible to use a scalar field in such problems, by replacing the wave Maxwell equation by the Helmholtz equation.

Note that the condition of equality of the incoherent and interference components of backscattered radiation is fulfilled only for a monochromatic wave unbounded in the transverse direction, i.e. a wave with an infinite spatial

coherence length. Otherwise, if the distance between the entrance and exit points of a plane wave exceeds the coherence length, the contribution of a cyclic chain of scatterings is suppressed by a random phase difference between two different regions of spatial coherence.

As a result, the interference component $I^{(C)}(\boldsymbol{r}, t)$ for radiation with finite time and spatial coherence lengths has the form

$$I^{(C)}(\boldsymbol{r}, t) \sim \sum_{n=1}^{\infty} \int d\boldsymbol{r}_1 ... d\boldsymbol{r}_n \exp[-(z_1 + z_n)/l]$$

$$\times \prod_{j=1}^{n-1} \Lambda(\boldsymbol{r}_{j+1} - \boldsymbol{r}_j) p(\boldsymbol{q}_j) \exp[\mathrm{i}(\boldsymbol{k}_\mathrm{i} + \boldsymbol{k}_\mathrm{s})_\perp (\boldsymbol{r}_1 - \boldsymbol{r}_n)_\perp$$

$$- (ct - z_1 - z_n - R_n)^2 L_\mathrm{T}^{-2}] f[(\boldsymbol{r}_1 - \boldsymbol{r}_n)_\perp]. \qquad (5.4)$$

Figure 4 shows the angular dependences of the gain $E^{(\mathrm{CBS})} = 1 + I^{(C)}/I^{(L)}$ of low-coherent backscattering calculated for different spatial coherence lengths L_c in the case of cw radiation ($L_T \to \infty$). The parameters of the medium corresponded to those of the latex suspension [49, 50]: the mean free path $l = 54$ μm, transport length $l^* = l/(1 - \overline{\cos\theta}) = 207$ μm ($\overline{\cos\theta}$ is the scattering angle cosine averaged over the absorption cross section), and the wavelength $\lambda = 0.5$ μm. For these parameters the gain for an unbounded monochromatic wave is $E^{(\mathrm{CBS})} \approx 2$. However, the half-width W of the CBS peak was only 0.1 mrad and could not be detected even at very good angular resolution ~ 0.1 mrad. In the case of low-coherence radiation, the peak width considerably increases: we obtained $W = 1.7$ mrad for $L_c = 140$ μm and $W \approx 3$ mrad for $L_c = 70$ μm. As the spatial coherence length increased, the peak width decreased: for $L_c = l^*$ and $2l^*$, we obtained $W = 0.7$ and 0.5 mrad, respectively. When the spatial coherence length L_c was an order of magnitude greater than the transport length, the usual angular dependence of CBS was recovered in the form of a triangle peak with the half-width $W = 0.12$ mrad coinciding with the width $W \sim (4kl^*)^{-1}$ obtained in the diffusion approximation.

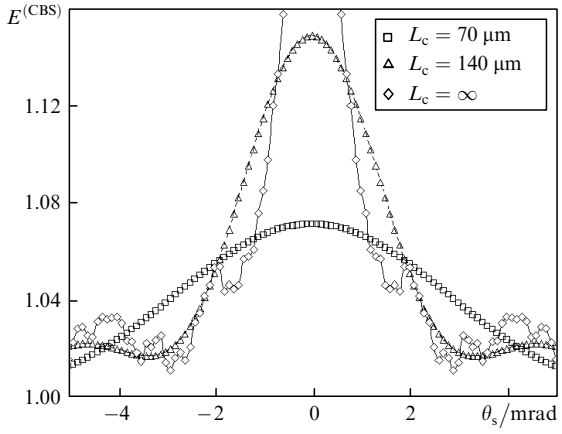

Figure 4. Dependences of the CBS peak $E^{(\mathrm{CBS})}$ on the scattering angle θ_s for cw incident radiation, $\Omega = 0$, for different spatial coherence lengths L_c. Optical parameters of the medium: $l = 54$ μm, $\overline{\cos\theta} = 0.74$; the wavelength is 0.5 μm.

Thus, for the values of parameters typical for biological systems at which the CBS peak of unbounded monochromatic radiation is virtually undetectable, the use of low-coherent radiation with the spatial coherence length smaller than the transport length makes it possible to increase the width of the CBS peak by one–two orders of magnitude. A large angular amplification range of backscattering, which is typical for low-coherent radiation, allows the use of the CBS effect for various applications and, first of all, in biomedical diagnostics [49, 50].

Note that in the case of low coherence, the gain is much lower than in the case of unbounded radiation and is $\sim 7\,\%$ of the incoherent component for $L_c = \frac{1}{3} l^* = 70$ μm and $\sim 15\,\%$ for $L_c = 140$ μm. Experimental data obtained for the model polystyrene suspension give the backscattering gain $\sim 5\,\%$ for $L_c = 140$ μm, which should be considered as good agreement, taking into account a limited angular resolution in the experiment.

We calculated the dependences of the coherent and incoherent components of a scattered ultrashort pulse on its delay time, which proved to be substantially different for these components. Figure 5 presents the calculated dependences of the backscattering gain $E^{(\mathrm{CBS})}$ on the delay time t of an ultrashort pulse for $L_c \approx 140$ μm and $L_T \approx 30$ μm, which corresponds to the pulse duration ~ 100 fs (parameters of the medium are as in Fig. 4). The calculations were performed taking into account contributions from different orders of scattering (up to $n = 1000$). One can see that for the given values of the scattering and transport lengths l and l^*, low-coherent backward scattering is produced by contributions of the first 8–10 scattering orders. Note also that to describe the interference component, it is not sufficient to take into account two-fold and three-fold scattering [82].

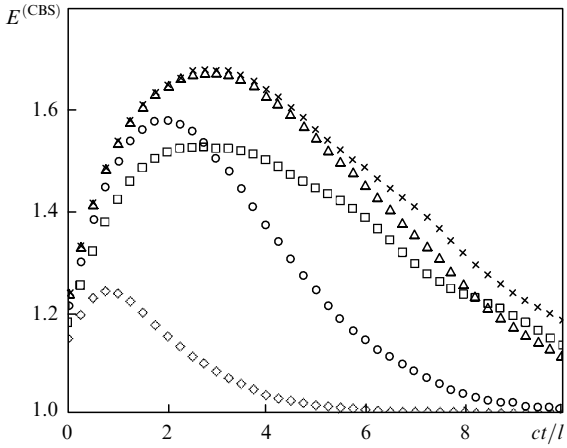

Figure 5. Dependences of the gain $E^{(\mathrm{CBS})}$ of low-coherent backscattering on the delay time of an ultrashort pulse in dimensionless units for $n = 2$ (◇), 5 (○), 10 (△) and 1000 (×): scalar field and $n = 1000$ (□) electromagnetic field; $L_T = 30$ μm, $L_c = 140$ μm, optical parameters are as in Fig. 4.

According to expressions for the incoherent and coherent components of scattered radiation, the pulse delay time is proportional to the optical path. In turn, the propagated path is proportional to the number $n \approx ct/l$ of scattering events. The presence of maxima of the time dependences in Fig. 5 indicates that, unlike CBS for cw radiation, which is

caused by the diffusion contribution of higher orders, low-coherent backward scattering is mainly determined by low-order scattering. It is this fact that determines the increase in the width of the backscattering cone. The localisation of the region of formation of the interference backscattering component of low-coherent radiation allows one to detect contributions to scattered radiation resolved over the penetration depth in turbid media and, in particular, to perform diagnostics in surface layers of biological tissues [45–47, 83].

Figure 6 presents the angular dependences of the interference gain of low-coherent radiation for different delays of a scattered ultrashort pulse. One can see that the interference component achieves its maximum when the delay time corresponds to the optical path equal to the transport length: $t = l^*/c$. For the chosen anisotropy parameter $\overline{\cos\theta}$, this corresponds approximately to the photon path with four scattering events. In this case, the gain $E^{(\mathrm{CBS})}$ is close to two, i.e. it is almost the same as that for cw coherent radiation. For $t > 5l^*/c$, no interference amplification of backscattered radiation is observed. Similar angular dependences for scattered 100-ps pulses were obtained in the CBS study of biological tissues [48]. Somewhat longer delay times (~ 4 ps) are probably explained by larger values of the transport length determined by fitting by the theoretical expression describing CBS in the diffusion approximation [68]. Note the diffusion approximation is obviously invalid for the calculation of low-coherent backward scattering.

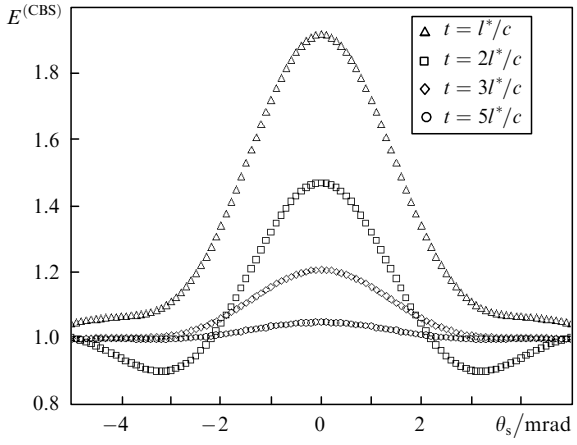

Figure 6. Angular dependences of the low-coherent backscattered component for an ultrashort pulse for different delay times.

6. Conclusions

Both cyclic diagrams describing the interference component of backward scattering [18, 68] and diagrams describing field correlations [13] in the theory of coherent and correlation effects of multiple scattering can be transformed to ladder diagrams. This allows these effects to be considered by using the corresponding Bethe–Salpeter equation. The formal difference from the initial ladder diagrams describing the transfer of the main, incoherent component of scattered radiation consist in the introduction of additional factors to the ladder diagram vertices. These factors determine the phase shift of the fields entering the definition of the propagator of the Bethe–Salpeter equation. By comparing the representation of this equation in the form of a series of ladder diagrams and simulations of random paths, we have shown that the consideration of phase relations in the stochastic simulation is also reduced to the addition of corresponding factors to each scattering event experienced by a photon propagating along a random path.

The Monte-Carlo method allows one to compare directly numerical results with theoretical predictions at each simulation step. The semianalytic method developed in our paper allows one to combine numerical simulations with the analytic approach used at large distances where theoretical results are obviously correct. The possibility of such a comparison considerably reduces the simulation time (by more than two orders of magnitude) by using analytic results instead of numerical ones at large distances between the entrance and exit points of radiation.

Our analysis has shown that scattering is really multiple only when the radiation intensity is calculated in a non-absorbing semi-infinite medium. In all other cases, the weight factors of the type $\exp(-D_s\overline{q^2}t) = \exp[-2(t/\tau) \times (l/l^*)]$ are used after each scattering event to simulate numerically time fluctuations with the diffusion decay of fluctuations or of the type $kl\sin\theta_s$ for CBS resulting in a rapid decay of a wave packet. Both the theory and numerical simulations become invalid because the contribution of non-ladder diagrams proves to be comparable with that of ladder diagrams. We have shown that the main assumption of the stochastic method in the simulation of radiation transfer in a strongly inhomogeneous medium that the distribution of the photon mean free path is described by the Poisson law is equivalent to the ladder approximation. However, even for small values of parameters $D_s\overline{q^2}t = 2(t/\tau)(l/l^*)$ or $kl\sin\theta_s$ in the case of a strong anisotropy of the phase function ($1 - \overline{\cos\theta_s} \ll 1$), the decrease rate of coherent effects proves to be much higher because it is determined by parameters t/τ and $kl^*\sin\theta_s$.

Multiple scattering, including coherent effects, is usually described in terms of a scalar field. As follows from our paper, the consideration of the electromagnetic nature of light results in a substantially different description of backscattering compared to the scalar-field description because in this case a great part of scattered radiation is formed by contributions from lower-order scatterings. Thus, the decrease rate of the TCF of the polarised component is considerably smaller, while that of the depolarised component is much larger than the decrease rate in the case of nonpolarised light. Note that the latter virtually coincides with the decrease rate in the scalar case. The polarised component of backscattered light is almost twice as large as the depolarised component.

The simulation method developed in the paper allows one to estimate the number of scattering events of light propagated through a layer in a strongly inhomogeneous turbid medium from the value of residual polarisation. Compared to the measurements of attenuation of non-polarised light, this gives additional information which can be used for determining the transport length. A comparative analysis considerably simplifies the simulation of radiation transfer and coherent effects in random strongly scattering media such as liquid crystals, biological tissues, etc. and also considerably expands applications of these methods.

Acknowledgements. This work was supported by the Russian Foundation for Basic Research (Grant No. 0-02-16577), the British Biotechnology and Biological Scientific Research Council (BBSRC, Project code BBS/B/04242), and the Royal Society (Grant No. 15298).

References

1. Stark H., Lubensky T.C. *Phys. Rev. E*, **55**, 514 (1997).
2. Special issue: Photon Correlation and Scattering. *Appl. Opt.*, **40**, 3965 (2001).
3. Harden J.L., Viasnoff V. *Curr. Opin. Colloid. Interface Sci.*, **6**, 438 (2001).
4. Gun'ko V.M., Klyueva A.V., Levchuk Y.N., Leboda R. *Adv. Colloid. Interface*, **105**, 201 (2003).
5. Van Tiggelen B.A., Skipetrov S.E. *Wave Scattering in Complex Media: From Theory to Applications* (Dordrecht: Kluwer Acad. Publ., 2003).
6. Priezzhev A.V., Tuchin V.V., Shubochkin L.P. *Lazernaya diagnostika v biologii i meditsine* (Laser Diagnostics in Biology and Medicine) (Moscow: Nauka, 1989).
7. Yodh A., Chance B. *Phys. Today*, **10**, 34 (1995).
8. Tuchin V.V. *Handbook of Optical Biomedical Diagnostics* (Washington: SPIE Press, 2002).
9. Tsang L., Ishimaru A. *J. Opt. Soc. Am. A*, **2**, 1331 (1985).
10. Van Albada M.P., Lagendijk A. *Phys. Rev. Lett.*, **55**, 2692 (1985).
11. Wolf P.E., Maret G. *Phys. Rev. Lett.*, **55**, 2696 (1985).
12. Feng S., Kane C., Lee P.A., Stone A.D. *Phys. Rev. Lett.*, **61**, 834 (1988).
13. Stephen M.J. *Phys. Rev. B*, **34**, 7564 (1986).
14. Fishkin J.B., Gratton E. *J. Opt. Soc. Am. A*, **10**, 127 (1993).
15. Lyubimov V.V. *Opt. Spektrosk.*, **80**, 687 (1996).
16. Barabenkov Yu.N. *Izv. Vyssh. Uchebn. Zaved. Ser. Radiofiz.*, **16**, 88 (1973).
17. Barabenkov Yu.N., Ozrin V.D. *Zh. Eksp. Teor. Fiz.*, **94**, 56 (1988).
18. Golubentsov A.A. *Zh. Eksp. Teor. Fiz.*, **86**, 47 (1984).
19. Cummins H.Z., Pike E.R. *Photon Correlation and Light Beating Spectroscopy* (New York: Plenum Press, 1973).
20. Lebedev A.D., Levchuk Yu.N., Lomakin A.V., Noskin V.A. *Lazernaya korrelyatsionnaya spektroskopiya v biologii* (Laser Correlation Spectroscopy in Biology) (Kiev: Naukova Dumka, 1987).
21. Protopopov V.V., Ustinov N.D. *Lazernoe geterodinirovanie* (Laser Heterodyning) (Moscow: Nauka, 1985).
22. Pecora R. *Dynamic Light Scattering: Application of Photon Correlation Spectroscopy* (New York: Plenum, 1985).
23. Maret G., Wolf E. *Zeitschrift fur Phys. B – Condensed Matter*, **65**, 409 (1987).
24. Pine D.J., Weitz D.A., Chaikin P.M., Herbolzheimer E. *Phys. Rev. Lett.*, **60**, 1134 (1988).
25. Weitz D.A., Pine D.J., in *Dynamic Light Scattering. The Method and Some Applications*. Ed. by W. Brown (New York: Oxford University Press, 1993) Ch. 16, p. 652.
26. Boas D.A., Cambell L.E., Yodh A.G. *Phys.Rev Lett.*, **75**, 1855 (1995).
27. Heckmeier M., Skipetrov S.E., Maret G., Maynard R. *J. Opt. Soc. Am. A*, **14**, 185 (1997).
28. Boas D.A., Meglinsky I.V., Zemany L., Cambell L.E., Chance B., Yodh A.G., in *SIC Selected Papers: Coherence Domain Methods in Biomedical Optics*. Ed. by V.V. Tuchin (Washington: SPIE Press, 1996) Vol. 2732, p. 34.
29. Skipetrov S.E., Meglinski I.V. *Zh. Eksp. Teor. Fiz.*, **113**, 1213 (1998).
30. Skipetrov S.E., Chesnokov S.S. *Opt. Atmos. Okean.*, **10**, 1493 (1997).
31. Kravtsenyuk O.V., Kuzmin V.L., Lyubimov V.V., Meglinski I.V. *Opt. Spektrosk.*, **100**, 950 (2006).
32. Rudolph W., Kempe M. *J. Mod. Opt.*, **14**, 1617 (1997).
33. Meglinsky I.V., Boas D.A., Yodh A.G., Chance B. *OSA Proc.*, **2**, 195 (1996).
34. Boas D.A., Yodh A.G. *J. Opt. Soc. Am. A*, **14**, 192 (1997).
35. Meglinski I.V., Korolevich A.N., Tuchin V.V. *Biomed. Radioelektron.*, **10**, 37 (2000).
36. Cheung C., Culver J.P., Takahashi K., Greenberg J.H., Yodh A.G. *Phys. Med. Biol.*, **46**, 2053 (2001).
37. Culver J.P., Durduran T., Furuya D., Cheung C., Greenberg J.H., Yodh A.G. *J. Cereb. Blood Flow Metab.*, **23**, 911 (2003).
38. Durduran T., Yu G., Burnett M.G., Detre J.A., Greenberg J.H., Wang J., Zhou C., Yodh A.G. *Opt. Lett.*, **29**, 1766 (2004).
39. Li J., Dietsche G., Iftime D., Skipetrov S.E., Maret G., Elbert T., Rockstroh B., Gisler T. *J. Biomed. Opt.*, **10**, 044002 (2005).
40. Korolevich A.N., Meglinski I.V. *Bioelectrochemistry*, **52**, 223 (2000).
41. Fercher A.F., Drexler W., Hitzenberger C.K., Lasser T. *Rep. Prog. Phys.*, **66**, 239 (2003).
42. Kemke M., Genack A.Z., Rudolph W., Dorn P. *J. Opt. Soc. Am. A*, **14**, 216 (1997).
43. Tuchin V.V. *Handbook of Coherent Domain Optical Methods* (Dordrecht: Kluwer Acad. Publ., 2004) Vol. 2.
44. Schmitt J.M. *IEEE J. Select. Topics Quantum Electron.*, **5**, 1205 (1999).
45. Bizheva K.K., Siegel A.M., Boas D.A. *Phys. Rev. E*, **58**, 7664 (1998).
46. Karamata B., Leutenegger M., Laubscher M., Bourquin S., Lasser T., Lambelet P. *J. Opt. Soc. Am. A*, **22**, 1380 (2005).
47. Wax A., Yang C., Dasari R.R., Feld M.S. *Appl. Opt.*, **40**, 4222 (2001).
48. Yoo K.M., Tang G.C., Alfano R.R. *Appl. Opt.*, **29**, 3237 (1990).
49. Kim Y.L., Liu Y., Turzhitsky V.M., Roy H.K., Wali R.K., Backman V. *Opt. Lett.*, **29**, 1906 (2004).
50. Kim Y.L., Liu Y., Turzhitsky V.M., Wali R.K., Roy H.K., Backman V. *Opt. Lett.*, **30**, 741 (2005).
51. Ospeck M., Fraden S. *Phys. Rev. E*, **49**, 4578 (1994).
52. Iwai T., Furukawa H., Asakura T. *Opt. Rev.*, **2**, 413 (1995).
53. Ishii K., Iwai T., Asakura T. *Opt. Rev.*, **4**, 643 (1997).
54. Eddowes M.H., Mills T.N., Delpy D.T. *Appl. Opt.*, **34**, 2261 (1995).
55. Skipetrov S.E., Chesnokov S.S. *Kvantovaya Elektron.*, **25**, 753 (1998) [*Quantum Electron.*, **28**, 733 (1998)].
56. Lenke R., Maret G. *Eur. Phys. J. B*, **17**, 171 (2000).
57. Lenke R., Tweer R., Maret G. *J. Opt. A – Pure Appl. Opt.*, **4**, 293 (2002).
58. Zimnyakov D.A., Sinichkin Yu.P., Kiseleva I.V., Agafonov D.N. *Opt. Spektrosk.*, **92**, 831 (2002).
59. Kuzmin V.L., Meglinski I.V. *Pis'ma Zh. Eksp. Teor. Fiz.*, **79**, 139 (2004).
60. Kuzmin V.L., Meglinski I.V. *Opt. Spektrosk.*, **97**, 108 (2004).
61. Rojas-Ochoa L.F., Lacoste D., Lenke R., Schurtenberger P., Scheffold F. *J. Opt. Soc. Am. A*, **21**, 1799 (2004).
62. Meglinski I.V., Kuzmin V.L., Churmakov D.Y., Greenhalgh D.A. *Proc. Roy. Soc. A*, **461**, 43 (2005).
63. Amic E., Luck J.M., Nieuwenhuizen T.M. *J. Phys. I*, **7**, 445 (1997).
64. Van Rossum M.C.W., Nieuwenhuizen Th.N. *Rev. Mod. Phys.*, **71**, 313 (1999).
65. Kuzmin V.L., Aksenova E.V. *Zh. Eksp. Teor. Fiz.*, **123**, 923 (2003).
66. Gorodnichev E.E., Dudarev S.L., Rogozkin D.B. *Phys. Rev. A*, **144**, 48 (1990).
67. Mishchenko M.I. *J. Quantum Spectrosc. Radiat. Transfer*, **56**, 673 (1996).
68. Akkermans E., Wolf P.E., Maynard R. *J. Phys. (Fr.)*, **49**, 77 (1988).
69. Sobol' I.M. *Metod Monte-Karlo* (Monte-Carlo Method) (Moscow: Nauka, 1985).
70. Kuzmin V.L., Meglinski I.V., Churmakov D.Yu. *Opt. Spektrosk.*, **98**, 673 (2005).
71. Kandidov V.P. *Usp. Fiz. Nauk*, **166**, 1309 (1996).
72. Kuzmin V.L., Meglinski I.V., Churmakov D.Yu. *Pis'ma Zh. Eksp. Teor. Fiz.*, **128**, 30 (2005).
73. Kuzmin V.L., Romanov V.P. *Usp. Fiz. Nauk*, **166**, 247 (1996).
74. Carney P.S., Wolf E., Agarwal G.S. *J. Opt. Soc. Am. A*, **14**, 3366 (1997).

75. Ishimaru A. *Wave Propagation and Scattering in Random Media* (New York: Academic Press, 1978; Moscow: Mir, 1981) Vols 1 and 2.
76. Gorodnichev E.E., Dudarev C.L., Rogozkin D.B. *Zh. Eksp. Teor. Fiz.*, **96**, 847 (1989).
77. MacKintosh F.C., John S. *Phys. Rev. B*, **40**, 2383 (1989).
78. MacKintosh F.C., Zhu J.X., Pine D.J., Weitz D.A. *Phys. Rev. B*, **40**, 9342 (1989).
79. Mishchenko M.I. *Phys. Rev. B*, **44**, 12597 (1991).
80. Mishchenko M.I., Luck J.M., Nieuwenhuizen T.M. *J. Opt. Soc. Am. A*, **17**, 888 (2000).
81. Kuzmin V.L. *Opt. Spektrosk.*, **93**, 482 (2002).
82. Gelikonov G.V., Dolin L.S., Sergeeva E.A., Turchin I.V. *Izv. Vyssh. Uchebn. Zaved., Ser. Radiofiz.*, **46**, 628 (2003).
83. Kim Y.L., Wali R.K., Roy H.K., Goldberg M.J., Kromin A.K., Chen K., Backman V. *IEEE J. Sel. Top. Quantum Electron.*, **9**, 243 (2003).